



Universidad Autónoma
de Madrid

Biblos-e Archivo
Repositorio Institucional UAM

Repositorio Institucional de la Universidad Autónoma de Madrid
<https://repositorio.uam.es>

Esta es la **versión de autor** del artículo publicado en:
This is an **author produced version** of a paper published in:

Applied Surface Science 509 (2020): 145118

DOI: <https://doi.org/10.1016/j.apsusc.2019.145118>

Copyright: © 2019 Elsevier B.V.

El acceso a la versión del editor puede requerir la suscripción del recurso
Access to the published version may require subscription

Controlled ultra-thin oxidation of Graphite promoted by cobalt oxides: influence of the initial 2D CoO wetting layer

C. Morales,^a D. Díaz-Fernández,^a R.J.O. Mossaneck,^b M. Abbate,^b J. Méndez^c, V. Pérez-Dieste,^d C. Escudero,^d J. Rubio-Zuazo,^{c,e} P. Prieto,^a and L. Soriano^{a,*}

^a *Departamento de Física Aplicada and Instituto de Ciencia de Materiales Nicolás Cabrera, Universidad Autónoma de Madrid, Francisco Tomás y Valiente 7, E-28049 Madrid, Spain*

^b *Departamento de Física, Universidade Federal do Paraná, Caixa Postal 19044, 81531-990 Curitiba, PR, Brazil*

^c *Instituto de Ciencia de Materiales de Madrid, ICMM-CSIC, Sor Juana Inés de la Cruz 3, E-28049 Madrid, Spain*

^d *ALBA Synchrotron, Carrer de la Llum 2-26, 08290 Cerdanyola del Vallès, Barcelona, Spain*

^e *BM25-SpLine ESRF, 71 Avenue des Martyrs, 38043 Grenoble, France*

^e *SpLine CRG BM25 Beamline, ESRF, BP 220, 6 rue Jules Horowitz, 38043 Grenoble, France*

* *Corresponding author: l.soriano@uam.es*

Keywords: CoO/HOPG interfaces, wetting layers, HOPG oxidation, x-ray photoemission spectroscopies, x-ray absorption spectroscopies.

Abstract:

The interaction of CoO with highly oriented pyrolytic graphite (HOPG) was studied using a set of complementary techniques. The morphology of the CoO thin film was determined using atomic force microscopy (AFM), whereas the electronic structure was investigated using x-ray absorption (XAS) and photoemission (PES) spectroscopies. The experimental spectra were analyzed using a configuration interaction CoO₆ cluster model calculation. The early stages of growth are characterized by the formation of a CoO wetting layer at the CoO/HOPG

interface. The electronic structure of the CoO wetting layer presents a clear 2D character, which is closer to the 2D HOPG substrate than to the 3D CoO bulk. This character of the wetting layer explains the posterior formation of CoO islands and excludes the alternative layer by layer growth mode. Further, the interaction between the CoO wetting layer and the outermost graphite layer favors the oxidation of the HOPG substrate which can be controlled by the thickness of the deposited CoO overlayer.

1. INTRODUCTION

The combination of cobalt oxides with carbon-based materials gives rise to important properties [1], leading to excellent performances in applications such as catalysts, biochemical sensors and cathodes for Li-ion batteries [2]. For instance, nano-sized cobalt oxides have demonstrated excellent behavior as negative electrode for Li-ion batteries [3], however the integrity of the electrode after many discharge and recharge cycles is not guaranteed. To overcome this problem, nanocomposites of cobalt oxides with graphene have been proposed as electrodes [4]. Also, cobalt nanoparticles are known to catalyze the formation of carbon nanotubes indicating a strong interaction of these materials [5]. Other interesting experiment involving cobalt oxides and graphite is the possibility of nano-patterning on highly oriented pyrolytic graphite (HOPG) with cobalt nanoparticles, via carbon gasification, at relatively low temperatures (400 °C), whereas other related works reported similar results at much higher temperatures (>800 °C). This was explained as due to the presence of a previously grown CoO ultra-thin layer, prior to its reduction to metallic Co nanoparticles, which produces a large number of defects at the HOPG surface [6,7]. In spite of the numerous applications of cobalt oxides and carbon-based materials, few fundamental studies have been done on these systems, and the mechanisms involved in the interaction of these materials remains unclear.

The growth of cobalt oxides on HOPG has already been studied. It was found that for low coverages, less than 50 equivalent monolayers, the main oxide is CoO with Co^{2+} chemical

species, whereas for larger coverages, the main component is Co_3O_4 which contains $\text{Co}^{2+}/\text{Co}^{3+}$ ions [8]. The growth mode was found to be of the Stranski–Krastanov mode, i.e. the formation of an initial CoO wetting layer followed by the growth of CoO islands. Other studies involving CoO/oxide interfaces have also been reported [9,10,11,12]. In general, cobalt oxides grow on other oxides in the form of CoO (Co^{2+}) using reactive thermal evaporation as the growth method. On the other hand, the growth in the form of the spinel Co_3O_4 ($\text{Co}^{2+}/\text{Co}^{3+}$) involves a more energetic growth method, such as oxygen plasma deposition [9]. Regarding the growth mode of CoO on other oxides, it depends mainly on the lattice mismatch of the oxide substrate with respect the CoO lattice. For instance, CoO grows in a Frank van der Merwe form, i.e. layer by layer mode, on Al_2O_3 and MgO , whereas it grows in a Volmer-Webber manner, i.e, islands mode, on SiO_2 [11].

The purpose of this paper is to study the interaction of ultra-thin-films of cobalt oxides deposited on a HOPG substrate at room temperature (RT). It is paid special attention to the physical/chemical interactions at the interface during the early stages of growth. The study involves both, the electronic structure of the CoO 2D overlayer as well as its effect on the HOPG substrate. To this end, we have grown cobalt oxides layers by reactive thermal evaporation of metallic cobalt in an oxygen atmosphere (2×10^{-5} mbar) at room temperature. We have used various x-ray spectroscopy techniques, with different probing depths, to characterize and analyze the chemical changes at the interface. In particular, the early stages of growth are characterized by the formation of a 2D-CoO wetting layer, which influences the island growth mode of the CoO overlayers. We also show that the formation of the cobalt oxide wetting layer promotes the posterior oxidation of the HOPG substrate.

The results presented in this paper are divided in three sections. First, we make a brief summary of the growth of CoO on HOPG. Then, we present an analysis of the electronic structure of the CoO overlayers. Finally, we study the oxidation of the HOPG substrate after the CoO deposition.

2. EXPERIMENTAL AND METHODS

The *in situ* experiments and measurements presented in this work have been performed in three different vacuum chambers. One located in our laboratory for X-ray photoelectron spectroscopy (XPS) measurements, other located at the PM4 beamline at the BESSY II synchrotron from Helmholtz-Zentrum Berlin for X-ray absorption spectroscopy (XAS) measurements and other located at the CIRCE beamline (NAPP) from the ALBA synchrotron in Barcelona for near ambient pressure X-ray photoelectron spectroscopy (NAP-XPS) measurements. In all cases, metallic Co was evaporated using a Knudsen type evaporator in an oxygen atmosphere (2×10^{-5} mbar) at room temperature, working at very low constant evaporation rate to study in detail the early stages of growth. Successive evaporations were performed, being the sample analyzed after each step of growth with the corresponding characterization technique. The HOPG substrate (ZYB grade, supplied by Bruker) was cleaved in air immediately before introduction into the vacuum chamber. Then, it was submitted to thermal annealing at 400 °C under ultra-high vacuum conditions (below 2×10^{-8} mbar) to desorb possible adsorbed species. Also, a CoO single crystal from Mateck was used as reference for HAXPES measurements.

The XPS measurements were performed with a CLAM-4 MDC hemispherical electron analyzer from Thermo Fisher, using Mg K α radiation. The pass energy was set at 20 eV, giving an overall resolution of 0.9 eV. The energy scale was calibrated by using the C 1s peak at 284.3 eV [13]. The spectra have been fitted using the XPS Peak software, version 4.1.

XAS measurements were carried out at the PM4 beamline located at the BESSY II synchrotron of the Helmholtz Zentrum Berlin (HZB). This beamline is equipped with a plane grating monochromator giving an overall resolution of about 100 meV at 530 eV. The spectra were taken in the total electron yield mode by measuring the drain current from the sample and normalized with the I_0 current taken from a clean gold sample. This allowed us to correct the spectra from the absorption due to the contamination of the beamline optics.

In situ NAP-XPS measurements were performed at the BL24-CIRCE beamline of the ALBA synchrotron using the NAPP end station, equipped with a Phoibos 150 NAP electron analyzer, which ensures a pressure difference of nine orders of magnitude between detector and sample, allowing measurements at pressures up to 20 mbar. The overall resolution was estimated of around 0.2 eV with a photon energy of 500 eV, pass energy of 10 eV and 20 μm of exit slit.

The *ex situ* hard X-ray photoelectron spectroscopy (HAXPES) measurements were taken at the BM25-Spline beamline at the ESRF in Grenoble. The spectra were measured using a photon energy of 10 keV, thus the inelastic mean free path of the photoelectrons varies, as calculated using the Tanuma et al. [14] formula, from 115 Å to 173 Å, depending on the propagation medium, CoO and HOPG respectively. This beamline is equipped with a double crystal monochromator and a high voltage cylindrical sector electron analyzer (CSA300HV) [15,16]. This instrument, together with the high brilliance of the BM25 beamline, fulfils the technical requirements imposed by HAXPES. The overall energy resolution for the experiment was about 2.0 eV. The AFM images were obtained with a Nanotec AFM microscope in the non-contact dynamic (tapping) mode and analyzed with the WSxM software [17].

The x-ray core level photoemission calculations were performed using a standard cluster model [18]. The cluster consisted of a $(\text{CoO}_6)^{-10}$ octahedron, which is solved within the configuration interaction method. In this case, the ground state wave function is expanded in configurations beyond the simple ionic picture $|3d^n\rangle$, such as $|3d^{n+1}\underline{L}\rangle$, $|3d^{n+2}\underline{L}^2\rangle$, etc., where \underline{L} denotes a hole in the ligand (oxygen) band. The main parameters of this model are the charge transfer energy ($\Delta = 5.5$ eV), the d-d Coulomb repulsion energy ($U = 5.2$ eV), the p-d transfer integral ($pd\sigma = 1.3$ eV) and the crystal field ($10Dq = 0.7$ eV) [18]. The final state wave function is also obtained from the ground state by removing a core hole electron. The cluster model is

solved with exact diagonalization and the spectral weight is found using the sudden approximation [19].

The x-ray absorption simulations were done using full multiplet calculations [20]. The dipole transition energies and intensities are calculated with Slater integrals reduced to 80% of their atomic value to account for additional screening. In the case of Co 2p XAS, the calculation considers 2p-2p, 2p-3d and 3d-3d interactions, whereas for the case of O 1s XAS, the simulation can be done by switching off the 2p spin-orbit and the 2p-3d interaction. These transitions are then projected into octahedral (O_h) symmetry – in the case of bulk calculations, with a crystal field parameter $10Dq = 0.9$ eV, or into tetragonal (D_{4h}) symmetry – in the case of the wetting layer calculations, with the crystal field parameters $10Dq = 0.5$ eV, $Dt = 0.01$ eV and $Ds = 0.06$ eV. In all cases, the in-plane and out-of-plane contributions can be separated and/or weighted accordingly, depending on the incident angle of the XAS measurement.

3. RESULTS AND DISCUSSION

3.1. Growth of CoO on HOPG

As mentioned in the previous section, CoO grows on HOPG following a Stranski–Krastanov growth mode. This leads to the formation of an initial CoO wetting layer followed by the growth of CoO islands, as it can be seen in Figures 1a, 1b and 1c. The initial wetting layer, from the results in Figures 1a and 1b, has a thickness slightly larger than 4 Å, in agreement with the lattice constant of bulk CoO determined at 305 K ($a=4.2614$ Å) [21]. Finally, only when the CoO wetting layer has grown on HOPG, dendritic islands start developing upon the wetting layer, as observed in Fig. 1c.

This morphology and growth mode has also been confirmed by the inelastic peak shape (IPSA) method [22]. This non-destructive method is based on a quantitative description of the peak shape caused by the inelastic scattering of the emitted photoelectron and Auger peaks in XPS experiments. It allows for an estimation of the elemental in-depth profile of an adsorbate

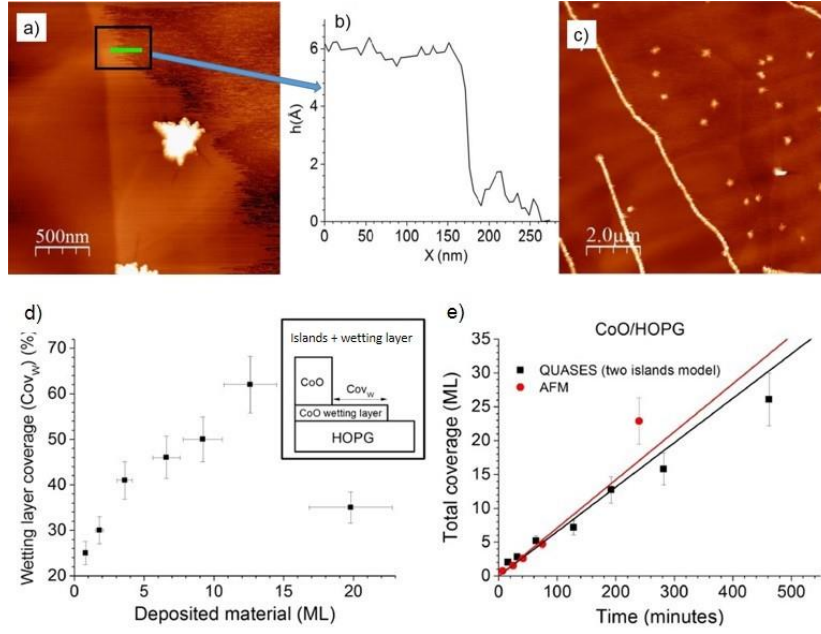


Figure 1: a) 2.5x2.5 μm² AFM image of the CoO/HOPG wetting layer; b) z-profile of the wetting layer, as indicated; c) 10x10 μm² AFM image of the wetting layer; d) wetting layer coverage as a function of the equivalent deposited material calculated by QUASES (see text); e) comparison of the total CoO equivalent coverage on HOPG as calculated from

on a substrate, being appropriate to study the morphology of the initial growth mechanisms of thin films. This method was implemented in the QUASES software [23], which takes into account the presence of an initial overlayer and the subsequent formation of islands on top of it. From this model, we calculated the portion of the wetting layer which is still uncovered by the CoO islands (Cov_w) as a function of the amount of deposited material, and the results are depicted in Figure 1d. For depositions up to around 12 equivalent monolayers (ML) of CoO, the wetting layer coverage – free of islands – grows monotonically, reaching about 60% of the total surface, finally dropping only when the amount of deposited material is larger than 15 ML. These results have also been compared to those obtained directly from the AFM images for each step of growth, as shown in Figure 1e, which displays an excellent agreement between both techniques.

3.2 Electronic structure of the CoO wetting layer

We shall begin the study of the electronic structure of the wetting layer by analyzing the x-ray Co 2p photoemission spectra as a function of the CoO coverage. The electronic structure of CoO in this particular core level has been widely investigated [24], and it is formed of many structures, mainly due to final state multiplet splitting, charge transfer satellites and plasmon loss structures [25]. However, since these features are very sensitive to the local environment of the Co atoms, the detailed analysis of these structures can give valuable information on the growth process.

To this end, the Co 2p XPS spectrum for CoO has been theoretically simulated with cluster model calculations of a Co^{2+} ion in octahedral symmetry [24,26]. The standard result for CoO is depicted in the upper panel of Figure 2a, labeled as bulk. The spectrum shows a main line, as well as a weak multiplet peak and a charge transfer satellite located at around 3 and 6 eV, respectively, from the main line. In order to simulate a loss of covalence due, for instance, to disorder or bi-dimensional character of the structure, Figure 2a also shows calculations where the $pd\sigma$ and $10Dq$ parameters have been intentionally lowered (labels s1, s2, s3 in Fig. 2a), as these parameters account for the hybridization level between Co 3d and O 2p orbitals ($pd\sigma$), and for the octahedral crystal field ($10Dq$) effect. As summarized in Figure 2b, the overall reduction of the covalence in CoO produces a decrease of the separation of the charge transfer satellite with respect to the main line (ΔE_{sat}), as well as an increase of the relative intensity of the charge transfer satellite ($I_{\text{sat}}/I_{\text{main}}$).

Then, the experimental Co 2p $3/2$ XPS spectra, for each step of growth, were fitted using the three peaks mentioned above, where their position and intensity were left as free parameters. This fitting procedure also included a Shirley background subtraction. Figure 2c presents the experimental Co 2p XPS spectra for some of the stages of growth and their respective fitting. The results obtained from these fittings, in particular the binding energy of the main line and the satellite energy separation (ΔE), as a function of the deposited material, are summarized in

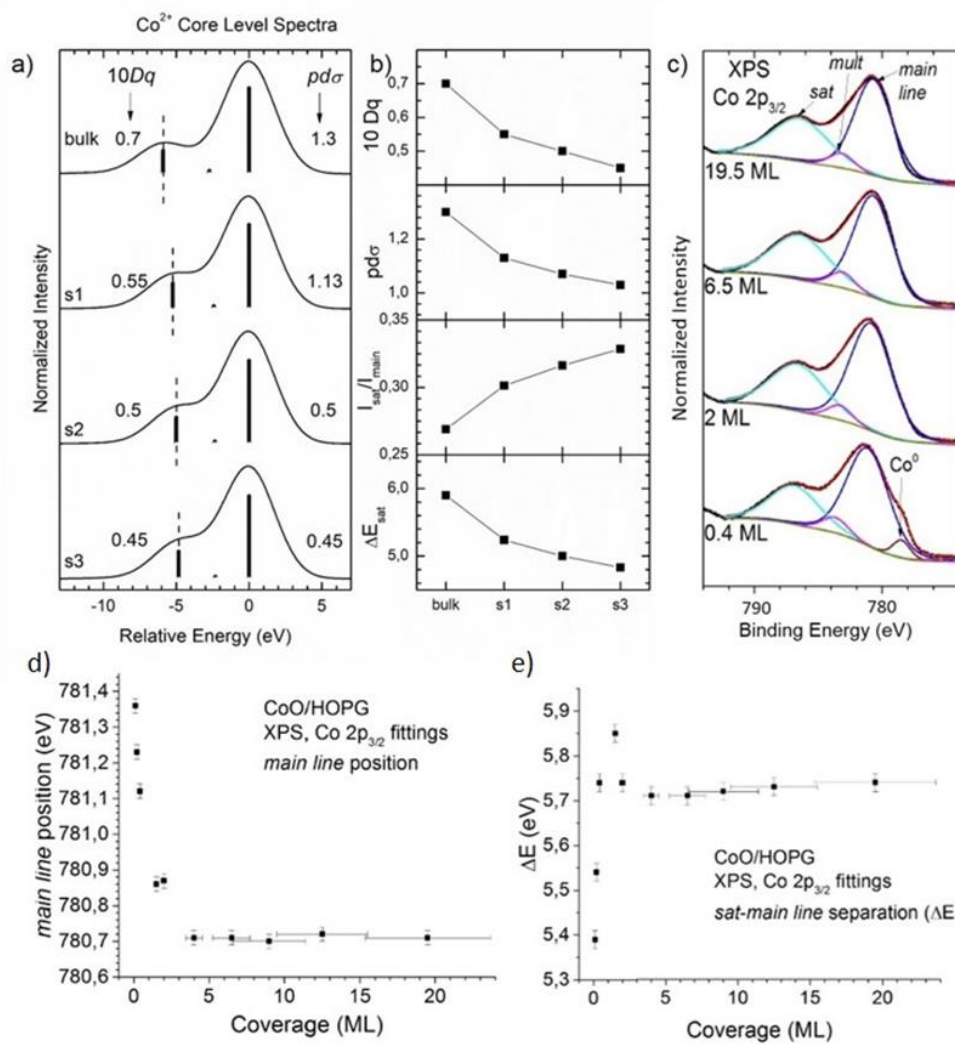


Figure 2: a) Cluster model calculations of the Co 2p $3/2$ XPS peak for different values of the $pd\sigma$ and $10Dq$ parameters. b) Main line-satellite energy separation (ΔE_{sat}) and relative intensity (I_{sat}/I_{main}) for the different values of $pd\sigma$ and $10Dq$ parameters; c) fittings of the experimental Co 2p XPS spectra using the peaks given by the calculations; d) binding energy position of the main line of the Co 2p XPS spectra as a function of the coverage; e) main line-satellite energy separation (ΔE_{sat}) as a function of the coverage.

Figures 2d and 2e. For very low coverages, i.e. during the formation of the wetting layer, the binding energy of the main line is progressively decreasing down to the normal value for bulk CoO (780.7 eV). This effect has been usually assigned to size effects in transition metal oxide ultra-thin films [12,27] and nanoparticles [28]. As for the energy separation of the satellite versus coverage, the values corresponding to the formation of the wetting layer are quite low with respect to those for larger coverages. Consequently, according to the above calculations, these results seem to indicate a loss of covalence of the initial CoO wetting layer formed on the

HOPG substrate. This effect can be attributed to the low dimensional character of the wetting layer, as well as due to the interaction with the HOPG substrate. As final note, for coverages below 1 Eq-ML a small shoulder at ~ 779.0 eV appears. This contribution is assigned to some metallic Co which still remains unoxidized at the CoO clusters located at the HOPG steps, in agreement with other published data [8, 29], thus they do not significantly affect to the formation of the wetting layer.

The previous description is a first indication that the electronic structure of the CoO wetting layer might differ from its bulk counterpart. Then, it seems worthy to study the electronic structure of the wetting layer, in more detail, XAS. Some specific properties of XAS, in particular its dependence with the photon polarization, which provides strong sensitivity to the incident angle, and the high sensitivity to the chemical environment of the ion, allow for a detailed study of anisotropic low-dimensional systems. Therefore, we have measured the Co 2p and O 1s XAS spectra of two samples: (i) 2 ML CoO/HOPG, representing the CoO wetting layer, and (ii) 20 ML CoO/HOPG, exemplifying the bulk CoO.

Figure 3a shows the Co 2p XAS spectrum for the 20 ML CoO/HOPG system. The experimental result is identical to previous bulk CoO results in the literature [30,31], presenting the Co 2p_{3/2} and Co 2p_{1/2} edges, split due to spin-orbit effects, whilst each edge is composed of different structures. It is worth noting that the experiment was performed at different incident angles, however the spectral shape is all similar, showing an isotropic character. The theoretical spectrum, also shown in Figure 3a, reproduces well the energy position and relative intensities of all the features in the experiment. This calculation is done by assuming a Co²⁺ ion in octahedral (O_h) symmetry and by computing the dipole transitions from 2p levels to empty 3d states [19]. In this symmetry, the Co 3d levels are split, by the crystal field, into the t_{2g} and e_g states (see Figure 3b), and so there would be no expected anisotropy between in-plane or out-of-plane states.

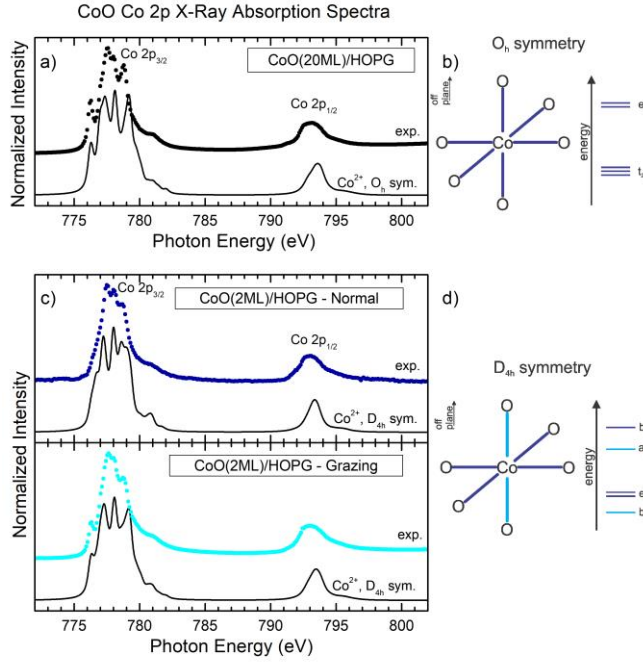


Figure 3: a) Experimental (dots) and calculated (line) Co 2p XAS spectra for 20 ML of CoO/HOPG. The simulated spectrum has been calculated in octahedral O_h symmetry; b) energy levels diagram of the Co 3d electronic states in octahedral (O_h) symmetry; c) experimental (dots) and calculated (line) Co 2p XAS spectra for 2 ML of CoO/HOPG. The experimental spectra have been taken at normal (upper panel) and grazing (bottom panel) photon incidence and the simulated spectra are calculated in tetragonal (D_{4h}) symmetry (see text); d) energy diagram of the Co 3d electronic states in tetragonal (D_{4h}) symmetry.

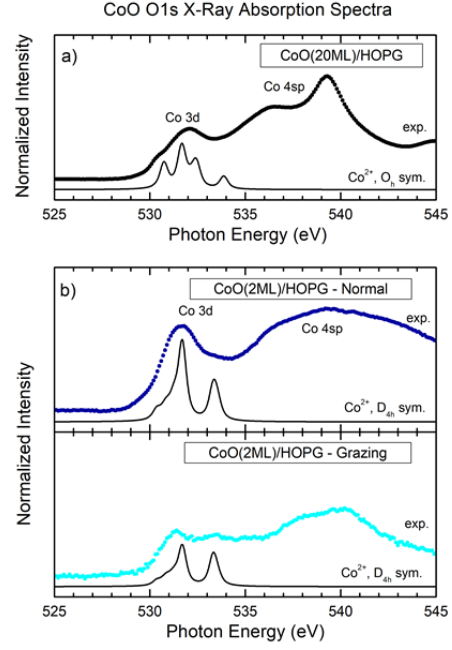


Figure 4: Experimental and calculated O 1s XAS spectra for: a) 20 ML of CoO/HOPG. The simulated spectrum has been calculated in octahedral (O_h) symmetry; b) 2 ML of CoO/HOPG. The experimental spectra have been taken at normal and grazing photon incidence and the spectrum is calculated in (D_{4h}) symmetry.

On the other hand, Figure 3c presents the Co 2p XAS spectra for the 2 ML CoO/HOPG compound, obtained in the normal ($\theta = 0$, top panel) and grazing ($\theta = 60^\circ$, bottom panel) incidence conditions. In normal incidence, in-plane States are excited by the photon electric field, whereas in grazing incidence, the out-of-plane states are preferably selected. The two experimental spectra are distinct from one another, as well as being different from the bulk one. The theoretical spectra, also shown in Figure 3b, is now obtained by assuming a Co^{2+} ion in tetragonal (D_{4h}) symmetry and by calculating the in-plane and out-of-plane dipole transitions from 2p levels to empty 3d states. Once again, it reproduces well the energy position and relative intensities of all the features in the spectrum. Now, in the tetragonal symmetry, the anisotropy arises due to the Co 3d levels being split into b_{1g} , e_g (in-plane), a_{1g} and b_{2g} (out-of-plane) states (see Figure 3d). It is worth mentioning that the CoO wetting layer spectra were reproduced with a smaller crystal field ($10Dq = 0.5$ eV) than in the CoO bulk case

($10Dq = 0.9$ eV) [32]. This is consistent to the effects of the loss of covalence observed in the Co 2p XPS spectra, as explained previously.

The same analysis can be made using the O 1s edge. The XAS spectrum for the 20 ML CoO/HOPG system is presented in Figure 4a. The structures in the experimental spectrum are related to the empty O 2p band, covalently mixed to Co 3d and Co 4sp states, which are similar to previous bulk CoO results [33]. The corresponding Co 3d region of the experimental spectrum is compared to the calculation of a Co^{2+} ion, in octahedral symmetry, which reproduces the energy position and relative intensities of the different features. Once again, this spectrum does not present any anisotropy, as in the case of the Co 2p edge.

In contrast, Figure 4b presents the O 1s XAS spectra for the 2 ML CoO/HOPG system, obtained in the normal ($\theta = 0$, top panel) and grazing ($\theta = 60$, bottom panel) incidence conditions. The experimental data indicate an anisotropic electronic structure, outlined by the clear difference in the relative intensity of the structures in the Co 3d region of the spectra. The theoretical spectra, in this case, are obtained by assuming a Co^{2+} ion in tetragonal (D_{4h}) symmetry and considering the in-plane and out-of-plane dipole transitions. Once again, it reproduces well the energy position and relative intensities of all the features in the spectra.

Then, the x-ray photoemission and absorption results indicate that the electronic structure of the wetting layer in the growth of CoO on HOPG is quite different from the corresponding bulk compound. It presents not only a less covalent nature, but also a highly anisotropic character in comparison to the usual material. These effects would be related to the low dimensionality of the wetting layer, as well as to the interaction with HOPG. This 2D electronic nature opposed to the bulk could be the reason why CoO grows in a Stranski–Krastanov fashion, as opposed to a layer-by-layer or island mode. The structural and electronic distortion of the wetting layer in contact with the graphite would prevent the growth of a new CoO layer, thus limiting the growth of CoO bulk islands only on the distorted CoO overlayer.

3.3 Analysis of the HOPG substrate

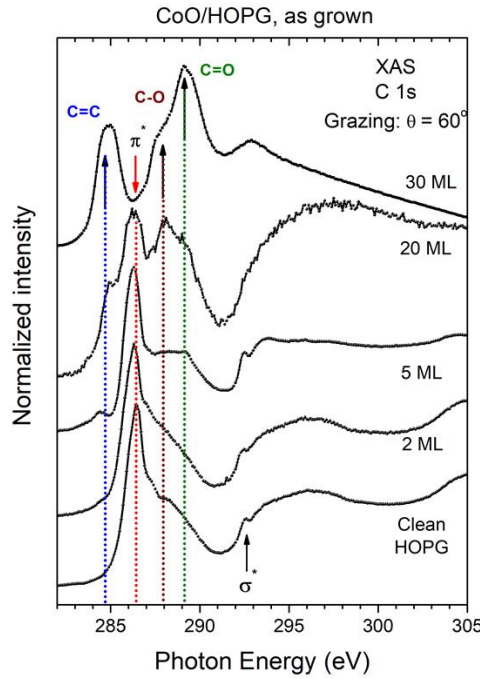


Figure 5: Experimental C 1s XAS spectra of the deposition of CoO on HOPG substrate for different coverages.

The effect on the electronic structure of HOPG, upon the deposition of CoO, is studied by examining the C 1s XAS spectra taken at different stages of growth. A typical C 1s XAS spectrum of HOPG reflects the anisotropy of its electronic structure, showing the π^* (off-plane) and σ^* (in-plane) states [34] with relative intensities depending on the photon incident angle. Because all the spectra shown in Figure 5 have been measured at grazing incidence angle ($\theta=60^\circ$), the spectrum for clean HOPG shows the typical asymmetric peak corresponding to the π^* states with the maximum at 286.0 eV, but the σ^* resonance appears as a weak structure starting at about 292.7 eV. For further deposition of CoO on the HOPG substrate, the spectra progressively change with three new peaks emerging in the energy range of the π^* states. These three peaks are clearly seen in the spectrum corresponding to the maximum coverage (30 ML), whereas the peak corresponding to the π^* states is suppressed. The peak located at 289.2 eV is assigned to the formation of C=O bonds, while the peak located at 288.0 eV is assigned to C-O bonds, in agreement with the literature [35,36,37,38]. In regards to the peak located at 284.5 eV, we assign it to the creation of broken carbon hexagons, thus leading to the formation of

C=C bonds as well as sp^3 defects at the HOPG surface. The above results clearly indicate that the CoO overlayer induces not only the oxidation of the carbon atoms, but also the creation of defects at the HOPG surface. Further, as the amount of deposited CoO increases, this effect becomes more pronounced.

In order to study the oxidation mechanism in more detail, we have also measured the C 1s photoemission peak of a 2 ML CoO/HOPG sample, grown *in situ* and submitted to oxidation under controlled oxygen atmosphere, in near ambient pressure condition. The main goal of this experiment was to observe whether the CoO wetting layer is able to inject oxygen to the HOPG substrate, as it is known that a clean HOPG surface under oxygen exposure at room temperature does not absorb a significant amount of oxygen [39]. The spectra have been taken at a photon energy of $h\nu = 380$ eV, at which the inelastic mean free path of the photoelectrons is restricted to a few monolayers. The results are shown in Figure 6a. First of all, the as grown 2 Eq-ML CoO/HOPG deposit shows a not modified C 1s spectrum compared to clean HOPG. This is in agreement with the XAS spectrum of Figure 5 for that coverage. On the other hand, two new peaks appear as the exposure to oxygen increases: one is located at about 288 eV and is assigned to C=O bonds, and the other at 286.0 eV is related to C-O bonds [40,41]. These results not only agree with those of XAS measurements for coverages above 2 Eq-ML, but also confirm that the presence of the wetting layer promotes the injection of oxygen to the HOPG surface. This is clearly seen in the spectra taken at an oxygen pressure of 1 mbar in Figure 6a, where these two peaks continuously grow upon time with oxygen exposure. It is also interesting to observe what is happening for very low oxygen exposures. The inset of Figure 6a shows, in detail, the energy region of these two peaks. The results show that for low oxygen pressure (10^{-3} mbar), C=O bonds are firstly formed, whereas C-O species grow significantly only at higher pressures (10^{-1} mbar). In general, the level of HOPG oxidation depends on two factors: the amount of CoO deposited and the exposure conditions (time and pressure) to O_2 . In this way it is important to take account that the thermal evaporation process

has a very low deposition rate, and therefore the highest coverages CoO/HOPG samples have been exposed to much more time to oxygen atmospheres during the growth compared to 2 Eq-ML samples. This fact increases the oxidation of the graphite, as shown in Figure 5.

In order to identify the effect of air exposure on the CoO/HOPG system, we have measured in our laboratory the C 1s XPS spectra of a sample containing 40 equivalent CoO ML. The measurements were done both, *in situ* immediately after its growth and *ex situ* after being exposed for one month to atmospheric pressure, so that the latter sample is supposed to be oxygen saturated. The spectra are compared to that of clean HOPG in Figure 6b. The C 1s spectrum for clean HOPG, shows a single asymmetric peak centered at 284.3 eV, which is assigned to the contribution of carbon atoms bounded under sp^2 hybridization [42]. The spectrum of the 40 CoO ML on HOPG grown *in situ* is broader than that of clean HOPG due to the presence of a new peak centered at 285.0 eV. This peak is usually assigned to carbon atoms with sp^3 hybridization [43], which, in our case, originates from broken carbon hexagons. This is in agreement with the results obtained with C 1s XAS spectra, in which the peak assigned to broken carbon hexagons dominates the final spectrum. The upper panels of Figure 6b show the C 1s XPS spectra for the sample containing 40 ML CoO/HOPG after one month exposed to air. This sample was measured at two different take off angles in order to vary the inelastic mean free path of the photoelectrons, thus allowing to distinguish the nearest surface region. In comparison to the spectra of *in situ* sample, there are two new peaks corresponding to C=O (288.5 eV) and C-O (286.0 eV) bonds in agreement with the

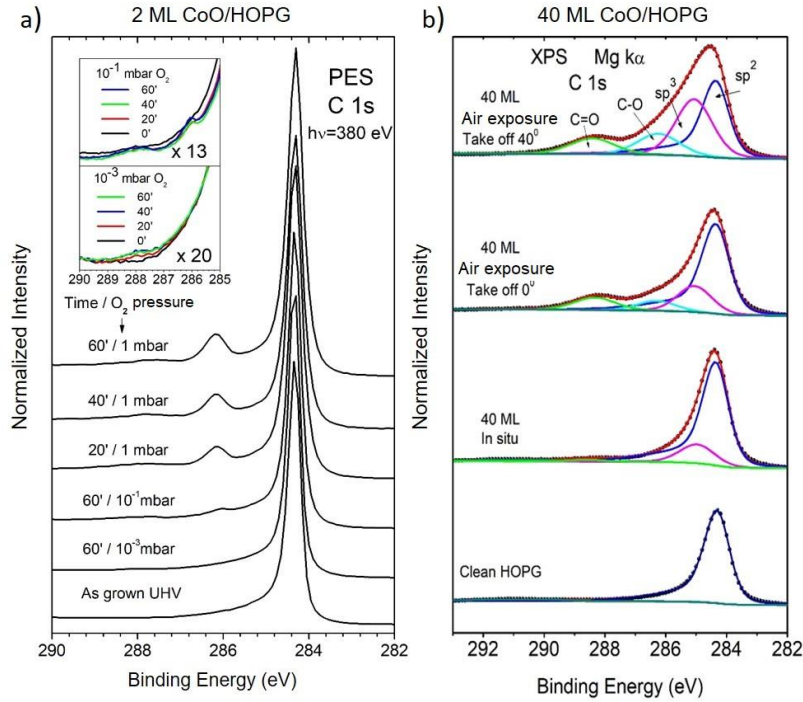


Figure 6: a) C 1s photoemission spectra of 2 ML CoO/HOPG measured at different oxygen pressures as labelled. The inset shows a detail for very low oxygen pressures; b) C 1s XPS spectra of a sample of 40 ML CoO/HOPG taken as grown in situ and after air exposition (superior panels).

photoemission measurements at higher pressures (Fig. 6a). The upper panel shows the spectrum of the air exposed sample taken at 40° take-off angle where the signal from the near surface region is enhanced. Indeed, the contribution corresponding to defects (sp³) and oxygen species increase significantly with respect to that of bulk graphite (sp²), indicating that both, C-O bonds and defects are mainly localized at the HOPG surface, i.e. at the CoO/HOPG interface.

Throughout this work we have presented different spectra obtained with surface techniques with a variety of probing depths. For instance, the mean probing depth of XAS is estimated to be about 50 Å [44], whereas for the photoemission spectra presented in Figure 6a this value is reduced to around 8 Å. However, in order to make an estimation of the thickness of the oxidized graphite layer, we would need a technique with a larger probing depth. That is because with the techniques already presented the signal coming from these oxygen atoms absorbed into the HOPG substrate would be superimposed to the signal of oxygen species present at the CoO wetting layer and islands.

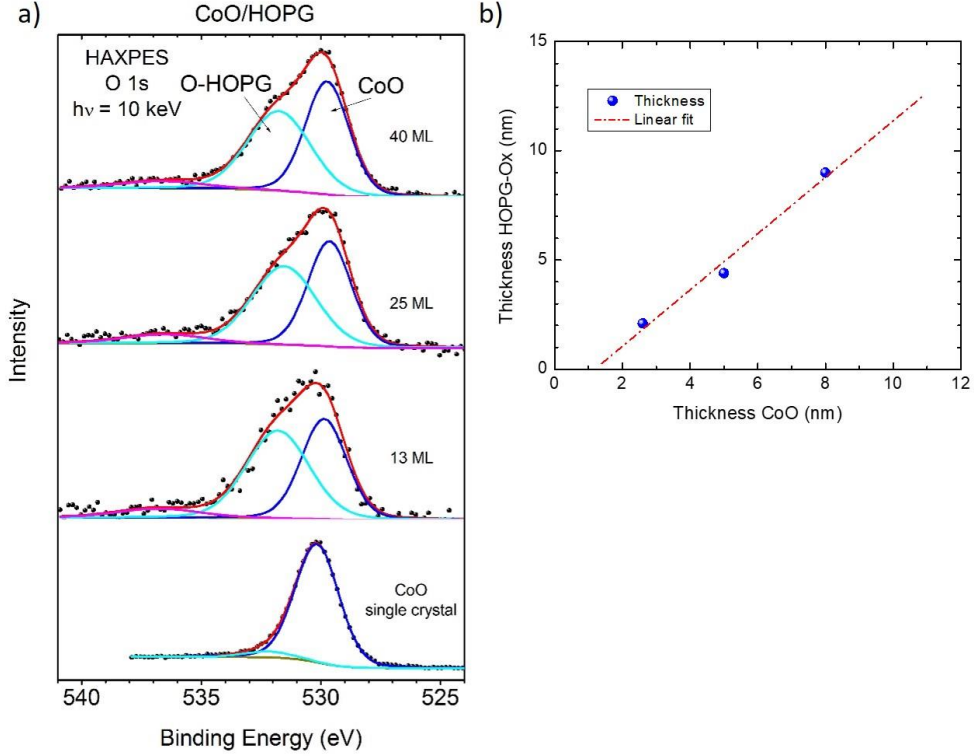


Figure 7: a) ex situ O 1s HAXPES spectra taken at 10 keV for three samples containing different coverages of CoO/HOPG and CoO single crystal; b) Thickness estimation of the oxidized graphite layer as a function of the CoO coverage as deduced from HAXPES intensities.

Therefore, we have also performed *ex situ* hard x-ray photoemission spectroscopy (HAXPES, at the Spline beamline in ESRF) measurements on three samples grown in our laboratory, containing 13, 25 and 40 equivalent ML of CoO/HOPG. Figure 7a shows the O 1s HAXPES spectra of the above samples. As stated before, the oxidation process is supposed to be saturated, thus the main two peaks appearing in the spectra at 530.0 eV and 531.9 eV are assigned to oxygen atoms from the CoO overlayer and oxygen atoms bounded to carbon atoms [45,46,47] respectively. The first peak agrees with that measured from a CoO single crystal sample, as shown at the bottom of Figure 7a. On the other hand, the peak corresponding to oxygen atoms bounded to carbon atoms (labeled as O-HOPG) conserves approximately its ratio with respect to that of CoO, independently of the CoO coverage. At a first glance, the amount of oxidized HOPG is proportional to the CoO coverage, in agreement with the previous XAS measurements.

Taking into account the thickness of the CoO equivalent layer and the fact that the oxidized HOPG layer lies below the last one, a simple approximation can be performed in order to estimate the thickness of the oxidized layer from the O-HOPG and CoO contribution intensities of the XPS O 1s spectra shown in Figure 7a. In this way, the theoretical intensities from the CoO and graphite oxide (HOPG-Ox) layers can be approximated as: [48]

$$I_{CoO} = I_{CoO}^{\infty} \left[1 - e^{-\frac{d_{CoO}}{\lambda_{CoO}^{CoO} \cos \theta}} \right] \quad (\text{Eq 1})$$

$$I_{HOPG_Ox} = I_{HOPG_Ox}^{\infty} \left[1 - e^{-\frac{d_{HOPG_Ox}}{\lambda_{HOPG_Ox}^{HOPG_Ox} \cos \theta}} \right] e^{-\frac{d_{CoO}}{\lambda_{HOPG_Ox}^{CoO} \cos \theta}} \quad (\text{Eq 2})$$

where λ_{CoO}^{CoO} is the IMFP of the CoO contribution at the CoO matrix, $\lambda_{HOPG_Ox}^{HOPG_Ox}$ the IMFP of the HOPG-Ox contribution at the oxidized graphite matrix and $\lambda_{HOPG_Ox}^{CoO}$ the IMFP of the HOPG-Ox contribution at the CoO matrix. By calculating the ratio I_{HOPG_Ox}/I_{CoO} , all the factors that form part of I_{CoO}^{∞} and $I_{HOPG_Ox}^{\infty}$ and depend on the electrons kinetic energy and other parameters from the analyzer can be avoided as they are the same for both CoO and oxidized HOPG. Further, the photon flux is obviously the same for both contributions and also the cross section and amount of oxygen atoms can be roughly approximated to be the same in both matrices. Therefore, the new equation from where the thickness can be estimated from the XPS fitting of Figure 3.7a is:

$$\frac{I_{HOPG_Ox}}{I_{CoO}} = \frac{\left[1 - e^{-\frac{d_{HOPG_Ox}}{\lambda_H^H \cos \theta}} \right] e^{-\frac{d_{CoO}}{\lambda_H^C \cos \theta}} \lambda_H^H}{\left[1 - e^{-\frac{d_C}{\lambda_C^C \cos \theta}} \right] \lambda_C^C} \quad (\text{Eq. 3})$$

where for $h\nu = 10$ keV, the IMPF are $\lambda_{HOPG_Ox}^{HOPG_Ox}$ ($E_{kin}=9468$ eV) ~ 17.3 nm, $\lambda_{HOPG_Ox}^{CoO}$ ($E_{kin}=9468$ eV) ~ 11.5 nm and $\lambda_C^C \sim \lambda_H^C$. Considering that the measurements were taken with an angle

$\theta=15^\circ$, and that 13, 25 and 40 Eq-ML correspond to 2.6, 5 and 8 nm, respectively, the estimation of the oxidized graphite as a function of the CoO coverage is shown in Figure 7b. Indeed, it can be seen the linear behavior of the thickness of the oxidized graphite layer with respect to the initial CoO layer thickness. The data show that the thickness of the oxidized graphite layer can be controlled by the thickness of the deposited CoO ultra-thin layer. These results could be very interesting in different applications involving carbon based materials such as the production of graphene oxide layers and graphene.

4. CONCLUSIONS

We studied the electronic structure of the wetting layer formed at the CoO/HOPG interface, as well as the effect of the CoO deposition on the HOPG substrate. The growth of CoO on HOPG begins by the deposition of a CoO wetting layer (this can be concluded from the analysis of AFM height profiles). This wetting layer forms a bridge between further CoO layers and the HOPG substrate; but its nature is closer to the 2D character of HOPG than to the 3D order of bulk CoO (this can be observed in the angular dependence of Co 2p and O 1s XAS). For this reason, additional layers of CoO tend to grow in islands, and not in a layer-by-layer mode (as observed in the analysis of the AFM data). The deposition of the CoO wetting layer also affects the outermost layer of HOPG (this can be seen in both the C 1s XAS and XPS). Interestingly enough, the interaction of the wetting layer at the interface favors the oxidation of the HOPG substrate (observed for larger CoO equivalent coverages in the C 1s XAS, as well as for exposition in air in the C 1s XPS and O 1s HAXPES spectra). The process starts with the creation of defects, i.e the breaking of the σ bonds between carbon atoms, leading to the absorption and diffusion of oxygen atoms. At oxygen saturation, the thickness of the final oxidized HOPG layer strongly depends on the thickness of the CoO ultra-thin overlayer, thus the oxidation of the HOPG can be directly controlled.

AUTHOR INFORMATION

Corresponding Author

*E-mail: l.soriano@uam.es

ORCID

Leonardo Soriano: 0000-0001-5715-376X

Notes

The authors declare no competing financial interest.

ACKNOWLEDGEMENTS

This investigation has been funded by the MINECO of Spain through the FIS2015-67367-C2-1-P project and by the Comunidad de Madrid through the NANOMAGCOSTCM-P2018/NMT4321 project. Authors R.J.O.M and M.A. thank the financial support of CNPq-Brazil. We thank HZB for the allocation of synchrotron radiation beamtime. Funding from the European Community's Seventh Framework Programme (FP7/2007-2013) under grant agreement n.º312284 is acknowledged. We thank the ALBA synchrotron staff for the successful performance of the CIRCE beam line during the NAP-XPS experiments. We acknowledge the Spanish MCIU and CSIC for financial support and for provision of synchrotron radiation facilities at BM25-SpLine at the ESRF. One of the authors (C.M.) thanks MCIU for a FPU grant. We also want to thank SEGAINVEX-UAM and SIdI-UAM for technical support.

REFERENCES

-
- [1] Linjie Zhi, Yong-Sheng Hu, Bassem El Hamaoui, Xuan Wang, Ingo Lieberwirth, Ute Kolb, Joachim Maier, Klaus Müllen. Precursor-Controlled Formation of Novel Carbon/Metal and Carbon/Metal Oxide Nanocomposites, *Adv. Mater.* 20 (2008) 1727-1731.
- [2] Xiao-Chen Dong, Hang Xu, Xue-Wan Wang, Yin-Xi Huang, Mary B. Chan-Park, Hua Zhang, Lian-Hui Wang, Wei Huang, Peng Chen. 3D Graphene-Cobalt Oxide Electrode for

High-Performance Supercapacitor and Enzymeless Glucose Detection *ACS Nano* 6 (2012) 3206-3213.

[3] P. Poizot, S. Laruelle, S. Grugeon, L. Dupont, J-M. Tarascon, Nano-sized transition-metal oxides as negative-electrode materials for lithium-ion batteries *Nature* 407 (2000) 496-499.

[4] Shubin Yang, Guanglei Cui, Shuping Pang, Qian Cao, Ute Kolb, Xinliang Feng, Joachim Maier, Klaus Müllen. Fabrication of Cobalt and Cobalt Oxide/Graphene Composites: Towards High-Performance Anode Materials for Lithium Ion Batteries *ChemSusChem* 3 (2010) 236-239.

[5] D.S. Bethune, C.H. Klang, M.S. de Vries, G. Gorman, R. Savoy, J. Vazquez, R. Beyers. Cobalt-catalysed growth of carbon nanotubes with single-atomic-layer walls. *Nature* 363 (1993) 605-607.

[6] D. Díaz-Fernández, J. Méndez, A. del Campo, R.J.O. Mossaneck, M. Abbate, M.A. Rodríguez, G. Domínguez-Cañizares, O. Bomati-Miguel, A. Gutiérrez, L. Soriano. Nanopatterning on highly oriented pyrolytic graphite surfaces promoted by cobalt oxides. *Carbon*, 85 (2005) 89-98.

[7] C. Morales, D.Díaz-Fernández, P.Prieto, Y.H.Lu, H.Kersell, A.delCampo ,C.Escudero ,V.Pérez-Dieste, P.Ashby, J.Méndez, L.Soriano. In situ study of the carbon gasification reaction of highly oriented pyrolytic graphite promoted by cobalt oxides and the novel nanostructures appeared after reaction. *Carbon* (2019) Accepted

[8] D. Díaz-Fernández, J.Méndez, O. Bomati-Miguel, F. Yubero, R.J.O. Mossaneck, M. Abbate, G. Domínguez-Cañizares, A. Gutiérrez, S. Tougaard, L. Soriano. The growth of cobalt oxides on HOPG and SiO₂ surfaces: A comparative study. *Surface Science* 624 (2014) 145-153.

[9] V.M. Jiménez, J.P. Espinós, A.R. González-Elipe. Control of the Stoichiometry in the Deposition of Cobalt Oxides on SiO₂ Surf. *Interface Anal.* 26 (1998) 62-71.

-
- [10] C.A.F. Vaz, D. Prabhakaran, E.I. Altman, V.E. Henrich. Experimental study of the interfacial cobalt oxide in $\text{Co}_3\text{O}_4/\alpha - \text{Al}_2\text{O}_3$ (0001) epitaxial films. *Phys. Rev. B* 80 (2009) 155457.
- [11] D. Díaz-Fernández, J. Méndez, F. Yubero, G. Domínguez-Cañizares, A. Gutiérrez, L. Soriano. Study of the early stages of growth of Co oxides on oxide substrates. *Surf. Interface Anal.* 46 (2014) 975-979.
- [12] D. Díaz-Fernández, E. Salas, J. Méndez, R.J.O. Mossaneck, M. Abbate, C. Morales, G. Domínguez-Cañizares, G.R. Castro, A. Gutiérrez, L. Soriano. Ultra-thin CoO films grown on different oxide substrates: Size and support effects and chemical stability. *Journal of Alloys and Compounds* 758 (2018) 5-13.
- [13] M. J. Webb, P. Palmgren, P. Pal, O. Karis, H. Grennberg. A simple method to produce almost perfect graphene on highly oriented pyrolytic graphite. *Carbon* 49 (2011) 3242-3249.
- [14] S. Tanuma, C. J. Powell, D. R. Penn. Calculations of electron inelastic mean free paths. V. Data for 14 organic compounds over the 50–2000 eV range. *Surf. Interf. Anal.* 21 (1994) 165-176.
- [15] J. Rubio-Zuazo, G.R. Castro. Hard X-ray photoelectron spectroscopy (HAXPES) (≤ 15 keV) at SpLine, the Spanish CRG beamline at the ESRF. *Nucl. Instrum. Method. Phys. Res. A* 547 (2005) 64-72.
- [16] J. Rubio-Zuazo, M. Escher, M. Merkel and G. R. Castro. High Voltage-Cylinder Sector Analyzer 300/15: A cylindrical sector analyzer for electron kinetic energies up to 15 keV. *Rev. Sci. Instrum.* 81 (2010) 043304.
- [17] I. Horcas, R. Fernández, J.M. Gómez Rodríguez, J. Colchero, J. Gómez Herrero, A.M. Baró. WSXM: A software for scanning probe microscopy and a tool for nanotechnology. *Rev. Sci. Instrum.*, 78 (2007) 013705.
- [18] A. Fujimori, F. Minami. Valence-band photoemission and optical absorption in nickel compounds. *Phys. Rev. B* 30 (1984) 957-971.

-
- [19] D. Alders, F. C. Voogt, T. Hibma, G. A. Sawatzky. Nonlocal screening effects in 2p x-ray photoemission spectroscopy of NiO (100). *Phys. Rev. B* 54 (1996) 7716-7719.
- [20] K. Okada, A. Kotani. Complementary Roles of Co 2 p X-Ray Absorption and Photoemission Spectra in CoO. *J. Phys. Soc. Jpn.* 61(1992) 449-453.
- [21] W. Jauch, M. Reehuis, H. J. Bleif, and F. Kubanek. Crystallographic symmetry and magnetic structure of CoO. *Phys. Rev. B* 64 (2001) 052102.
- [22] S. Tougaard, *J. Vac. Sci. Technol. A* 8 (1990) 2197.
- [23] S. Tougaard, QUASES. Software package for quantitative XPS/AES of Surface nanostructures by inelastic peak shape analysis, see: www.QUASES.com. (accessed: January 2019).
- [24] A.E. Bocquet, T. Mizokawa, T. Saitoh, H. Namatame, A. Fujimori. Electronic structure of 3d-transition-metal compounds by analysis of the 2p core-level photoemission spectra. *Phys. Rev. B* 46 (1992) 3771.
- [25] M.C. Biesinger, B.P. Payne, A.P. Grosvenor, L.W.M. Lau, A.R. Gerson, R.StC. Smart. Resolving surface chemical states in XPS analysis of first row transition metals, oxides and hydroxides: Cr, Mn, Fe, Co and Ni *Appl. Surf. Sci.* 257 (2011) 2717-2730.
- [26] G. van der Laan, C. Westra, C. Haas, G.A. Sawatzky. Satellite structure in photoelectron and Auger spectra of copper dihalides. *Phys. Rev. B* 23 (1981) 4369.
- [27] J.P. Espinós, G. Lassaletta, A. Caballero, A. Fernández, A.R. González-Elipé, A. Stampfl, C. Morant, J.M. Sanz. Synchrotron Photoemission Characterization of TiO₂ Supported on SiO₂. *Langmuir* 14 (1998) 4908-4914.
- [28] K. Borgohain, J.B. Singh, M.V. Rama Rao, T. Shripathi, S. Mahamuni. Quantum size effects in CuO nanoparticles. *Phys. Rev. B* 61 (2000) 11093.
- [29] National Institute of Standards and Technology; X-ray Photoelectron Spectroscopy (XPS) Database, 2013.

-
- [30] S. Ya. Istomin, O. A. Tyablikov, S. M. Kazakov, E. V. Antipov, A. I. Kurbakov, A. A. Tsirlin, de N. Hollmann, Y. Y. Chin, H.-J. Lin, C. T. Chen, A. Tanaka, L. H. Tjeng and Z. Hu. An unusual high-spin ground state of Co^{3+} in octahedral coordination in brownmillerite-type cobalt oxide. *Dalton Trans.*, 44 (2015) 10708-10713.
- [31] S. C. Wi, J.-S. Kang, J. H. Kim, S.-B. Cho, B. J. Kim, S. Yoon, B. J. Suh, S. W. Han, K. H. Kim, K. J. Kim, B. S. Kim, H. J. Song, H. J. Shin, J. H. Shim, B. I. Min. Electronic structure of $\text{Zn}_{1-x}\text{Co}_x\text{O}$ using photoemission and x-ray absorption spectroscopy. *Appl. Phys. Lett.* 84 (2004) 4233.
- [32] F. M. F. de Groot, M. Abbate, J. van Elp, G. A. Sawatzky, Y. J. Ma, C. T. Chen and F. Sette. Oxygen 1s and cobalt 2p X-ray absorption of cobalt oxides. *J. Phys.: Condens. Matter* 5 (1993) 2277-2288.
- [33] L. Soriano, M. Abbate, A. Fernández, A. R. González-Elipe, F. Sirotti, J. M. Sanz. Oxidation State and Size Effects in CoO Nanoparticles *J. Phys. Chem. B*, 103 (1999) 6676-6679.
- [34] D.A. Fischer, R.M. Wentzcovitch, R.G. Carr, A. Continenza, A.J. Freeman. Graphitic interlayer states: A carbon *K* near-edge x-ray-absorption fine-structure study. *Phys. Rev. B* 44 (1991) 1427-1429.
- [35] Y. Kebukawa, M.E. Zolensky, A. L. D. Kilcoyne, Z. Rahman, P. Jenniskens, G.D. Cody. Diamond xenolith and matrix organic matter in the Sutter's Mill meteorite measured by C-XANES *Meteoritics & Planetary Science* 49 (2014) 2095-2103.
- [36] G.D. Cody, E. Heying, C. M. O. Alexander, L.R. Nittler, A. L. D. Kilcoyne, S.A. Sandford, R.M. Stroud. Establishing a molecular relationship between chondritic and cometary organic solids *Proceedings of the National Academy of Sciences* 108 (2011) 19171.
- [37] H.-K. Jeong, L. Colakerol, M.H. Jin, P.A. Glans, K.E. Smith, Y.H. Lee. Unoccupied electronic states in graphite oxides. *Chemical Physics Letters* 460 (2008) 499-502.

-
- [38] H.-K. Jeong, H.-J. Noh, J.-Y. Kim, M. H. Jin, C. Y. Park, Y. H. Lee. X-ray absorption spectroscopy of graphite oxide. *EPL*, 82 (2008) 67004.
- [39] D.C. Sorescu, K.D. Jordan, P. Avouris. Theoretical Study of Oxygen Adsorption on Graphite and the (8,0) Single-walled Carbon Nanotube *J. Phys. Chem. B* 105 (2001) 11227-11232.
- [40] D. Yang, A. Velamakanni, G. Bozoklu, S. Park, M. Stoller, R.D. Piner, S. Stankovich, I. Jung, D.A. Field, C.A. Ventrice Jr., R.S. Ruoff, Chemical analysis of graphene oxide films after heat and chemical treatments by X-ray photoelectron and Micro-Raman spectroscopy. *Carbon* 47 (2009) 145-152.
- [41] K. Haubner, J. Murawski, P. Olk, L. M. Eng, C. Ziegler, B. Adolphi, E. Jaehne. The Route to Functional Graphene Oxide. *ChemPhysChem* 11 (2010) 2131-2139.
- [42] M.J. Webb, P. Palmgren, P. Pal, O. Karis, H. Grennberg. A simple method to produce almost perfect graphene on highly oriented pyrolytic graphite. *Carbon* 49 (2011) 3242-3429.
- [43] B. Rousseau, H. Estrade-Szwarckopf, A.-L. Thoman, P. Brault. Stable C-atom displacements on HOPG surface under plasma low-energy argon-ion bombardment. *Appl. Phys. A* 77 (2003) 591-597.
- [44] M. Abbate, J. B. Goedkoop, F. M. F. de Groot, M. Grioni, J. C. Fuggle, S. Hofmann, H. Petersen, M. Sacchi. Probing Depth of Soft X-ray Absorption Spectroscopy Measured in Total-electron-yield Mode. *Surface and Interface Analysis*, 18 (1992) 65-69.
- [45] Jean-Charles Dupin, Danielle Gonbeau, Philippe Vinatierb, Alain Levasseur. Systematic XPS studies of metal oxides, hydroxides and peroxides. *Phys. Chem. Chem. Phys.*, 2 (2000) 1319-1324.
- [46] Abhijit Ganguly, Surbhi Sharma, Pagona Papakonstantinou, Jeremy Hamilton. Probing the Thermal Deoxygenation of Graphene Oxide Using High-Resolution In Situ X-ray-Based Spectroscopies. *J. Phys. Chem. C* 115 (2011) 17009-17019.

-
- [47] C. Hontoria-Lucas, A.J. López-Peinado, J.D. López-González, M.L. Rojas-Cervantes, R.M. Martín-Aranda; Study of oxygen-containing groups in a series of graphite oxides: physical and chemical characterization; *Carbon*; 33 (1995) 1585-1592.
- [48] D. Briggs and M. P. Seach, *Practical Surface Analysis. Volume 1. Augr and X-ray Photoelectron Spectroscopy, second edition*; Weinheim, Germany; Wiley, 1990.

Figure Captions:

Figure 1: a) $2.5 \times 2.5 \mu\text{m}^2$ AFM image of the CoO/HOPG wetting layer; b) z-profile of the wetting layer, as indicated; c) $10 \times 10 \mu\text{m}^2$ AFM image of the wetting layer; d) wetting layer coverage as a function of the equivalent deposited material calculated by QUASES (see text); e) comparison of the total CoO equivalent coverage on HOPG as calculated from QUASES and AFM data.

Figure 2: a) Cluster model calculations of the Co 2p $3/2$ XPS peak for different values of the $pd\sigma$ and $10Dq$ parameters. b) Main line-satellite energy separation (ΔE_{sat}) and relative intensity ($I_{\text{sat}}/I_{\text{main}}$) for the different values of $pd\sigma$ and $10Dq$ parameters; c) fittings of the experimental Co 2p XPS spectra using the peaks given by the calculations; d) binding energy position of the main line of the Co 2p XPS spectra as a function of the coverage; e) main line-satellite energy separation (ΔE_{sat}) as a function of the coverage.

Figure 3: a) Experimental (dots) and calculated (line) Co 2p XAS spectra for 20 ML of CoO/HOPG. The simulated spectrum has been calculated in octahedral O_h symmetry; b) energy levels diagram of the Co 3d electronic states in octahedral (O_h) symmetry; c) experimental (dots) and calculated (line) Co 2p XAS spectra for 2 ML of CoO/HOPG. The experimental spectra have been taken at normal (upper panel) and grazing (bottom panel) photon incidence and the simulated spectra are calculated in tetragonal (D_{4h}) symmetry (see text); d) energy diagram of the Co 3d electronic states in tetragonal (D_{4h}) symmetry.

Figure 4: Experimental and calculated O 1s XAS spectra for: a) 20 ML of CoO/HOPG. The simulated spectrum has been calculated in octahedral (O_h) symmetry; b) 2 ML of CoO/HOPG. The experimental spectra have been taken at normal and grazing photon incidence and the spectrum is calculated in (D_{4h}) symmetry.

Figure 5: Experimental C 1s XAS spectra of the deposition of CoO on HOPG substrate for different coverages.

Figure 6: a) C 1s photoemission spectra of 2 ML CoO/HOPG measured at different oxygen pressures as labelled. The inset shows a detail for very low oxygen pressures; b) C 1s XPS spectra of a sample of 40 ML CoO/HOPG taken as grown in situ and after air exposition (superior panels).

Figure 7: a) ex situ O 1s HAXPES spectra taken at 10 keV for three samples containing different coverages of CoO/HOPG and CoO single crystal; b) Thickness estimation of the oxidized graphite layer as a function of the CoO coverage as deduced from HAXPES intensities.